Investigation of Droplet Size Distribution for Vibrating Mesh Atomizer

Pallavi Sharma
University of New Mexico
Mohammed Quazi
University of New Mexico
Irma Rocio Vazquez
University of New Mexico
Nathan Jackson (njack@unm.edu)
University of New Mexico

Research Article

Keywords: Ultrasonic, Vibrating mesh atomizer, MEMS, Volumetric median diameter, Span, Fine particle fraction, atomizer

Posted Date: November 30th, 2021

DOI: https://doi.org/10.21203/rs.3.rs-1108564/v1

Abstract

Vibrating mesh atomizers (VMA) are increasing in demand for various aerosol applications due to their ability to generate uniformly sized droplets. Currently there are two types of VMA (commercial metallic membranes and silicon based). High Uniformity and control of small droplet size are the basic requirements for many aerosol applications, for which ultrasonic or VMA are employed. However, there is limited research on understanding the droplet size distribution of different types of atomizers. In this study three aerosol generators were investigated: Ultrasonic, metallic VMA, and MEMS-based silicon VMA. The primary objective was to compare these devices on droplet size distribution and mechanism of action. A systematic study to compare the performance of the two VMA was investigated based on droplet distribution, volumetric median diameter (VMD) using liquids with different physiochemical properties. Size distribution of the droplet produced by the metallic VMA was twice the span compared to silicon VMA for fluids with viscosity <2cP. The metallic VMA also resulted in an increase in VMD as the viscosity increased, whereas the Si VMA did not see a significant increase in VMD. The silicon-based VMA demonstrated a 4-15x increase in fine particle fraction control compared to metallic VMA. The results demonstrate that silicon based VMA has narrower droplet distribution with more uniform droplet size and lower span compared to metallic VMA.

Introduction

Atomizers are very important due to their wide range of application areas such as drug delivery [1], spray coating [2], spin-spray deposition of thin films [3,4] spray drying [5], mass spectrometry [6], and many other applications. The aerosol droplet size and their distribution are some of the most critical parameters to determine the atomizers performance in these applications. The majority of applications are interested in producing small droplets (1-5 μm) with a very tight control of droplet sizes, thus the overall goal for developing new atomizers is to typically eliminate or reduce large droplets (>5 μm) and ultrafine droplets (<1 μm). For example, inhaled drug delivery requires small droplet size (1-5 μm) to deliver the drugs to the respiratory tract, whereas large droplets get deposited in the mouth or throat, and ultrafine particles can enter the bloodstream [7], where they can accumulate and cause various health issues. In agricultural pesticide spraying, droplets need to be small enough to cover the crop and not drift into air [8]. In pharmaceutical spray coating, droplets need to be large enough to coat the tablets but not too large to get wasted. For advanced or additive manufacturing small droplets typically results in increased resolution and thin film uniformity. Therefore, controlling and understanding the mechanisms associated with droplet size distribution is critical for atomizer performance. An atomizer is the device that is used to convert liquid into aerosol. Traditional atomizers use jet or air pressure and a baffle to form and filter droplets. First studies of droplet formation and disintegration from liquid were performed in 1954 [9] and since then more parameters have been investigated. Droplet characteristics and size distribution for twin flow nozzles have been studied [10], where the authors concluded that the spray atomization characteristics depended on gas to liquid mass flow rate ratio. Furthermore, [11] investigated the spray distribution of the pneumatic atomizers by beam steering correction in laser diffraction method.

Ultrasonic atomizers were developed to overcome the deficiencies of jet atomizers such as inhomogeneity of aerosols, low transport factor, use of air streams, high power consumption and numerous components making them bulky and importable. Ultrasonic atomizers use a piezoelectric transducer horn vibrating in the (0,1) mode at a high frequency and generate polydisperse droplets by the capillary wave mechanism. Ultrasonic atomizer work on the theory of Faraday excitation as shown in Figure 1(a) and uses high frequency oscillation to generate an aerosol. Actuated by piezoceramic transducer horn, ultrasonic waves are generated on the vibrating liquid, and the vibration peak formed by the amplitude separates and breaks the liquid from the surface creating the droplets. The ultrasonic atomizer in Figure 1(b), also known as mist generator, consists of a piezoelectric transducer that is submerged in liquid. Ultrasonic atomizers typically operate in the MHz range with high power of 1-100W and they typically have high flow rates. Extensive research has been investigated on effect of capillary waves and liquid physiochemical properties on droplet distribution of ultrasonic atomization [12–15]. The droplet breakup and aerosol formation depend on actuation frequency and property of the liquid, but this type of atomizer system has problems with settling of suspension, deterioration of heat sensitive materials, residual formation, expensive electronics, low output rate and production of non-uniform droplets.

New atomization methods have been developed within the past decade including a Fourier Horn [16], surface acoustic wave (SAW) [17], and vibrating mesh atomizers (VMA) [18]. A comparison study between commercial metallic VMA and SAW studying the droplet size recently demonstrated the advantages of VMA at controlling droplet size distribution [14]. VMA, also known as mesh atomizers, were developed primarily for inhaled drug delivery applications as an advancement on ultrasonic atomization method demonstrating improved efficiency, speed of atomization, low power consumption and controlled droplet distribution. VMA use a vibrating membrane with multiple apertures to produce droplets, their working principle is shown in Figure 1(c). The VMA membrane oscillates in the (0,2) or (0,3) acoustic mode as compared to ultrasonics which operate in the (0,1) mode (Figure 1(f and g)). Both devices are actuated using piezoelectric films, the VMA membrane typically vibrates at a frequency of approximately 100 kHz. During the positive cycle, pressure builds up in the liquid which is in contact with the mesh resulting in pushing the liquid through the aperture/nozzles and the reverse cycle contributes to pinching off the liquid on the outlet of the mesh causing atomization to occur. Typical commercial VMA consist of a metallic membrane as shown in Figure 1(d), and the nozzles are created by either laser drilling process or electroplating [19]. Commercial VMA typically use stainless steel membranes, but electroplated VMA have also used Pd-Ni or other alloys. Recently, Silicon-based VMA were developed using monolithic MEMS microfabrication techniques [3,4,20,21] shown in Figure 1(e). MEMS VMA devices were developed to increase yield, reduce cost, and add functionality through monolithic integration [20]. The MEMS VMA were designed to have similar dynamics as the metallic VMA, but the two devices have distinct differences due to the microfabrication methods such as: nozzle shape, membrane material properties (thermal, mechanical, and electrical), and surface wettability and roughness, which has resulted in different atomization properties such as droplet size distribution and liquid compatibilities.

Metallic VMA are extensively being researched for atomization rate [22], nozzle taper angle [23], and effect of operating parameters on its performance [24]. However, there is limited investigation on droplet size distribution and most research with VMA devices only investigate atomization of water. This paper focuses on understanding the parameters that affect droplet size distribution by systematically comparing metallic and silicon-based MEMS VMA. This paper investigates three types of atomizers, ultrasonic, metallic (stainless steel) VMA and MEMS based silicon VMA in regard to droplet size distribution using various liquids with different physiochemical properties. A detailed analysis of variance (ANOVA) design of experiments was used to determine key factors that influence droplet size and to compare performance of the metallic and silicon based VMA devices.

Methods:

The ultrasonic and metallic VMA were purchased from STEMiNC (Steiner and Martins Inc.). The ultrasound mist generator (SMUTK900LV110V, STEMiNC) operated at 1.7 MHz with 60 W power and high flow rate of 900 ml/Hr. Two types of stainless steel VMA were used with varying outlet nozzle size 10 µm (SMMOD20F113H10, STEMiNC) and 5 µm (SMMOD10F190, STEMiNC) and had a (0,2) resonant frequency mode of 113 kHz and 190 kHz respectively. The 10 µm outlet nozzle device was capable of dispensing 200 ml/Hr. The MEMS silicon based VMA was fabricated in a class 1000 cleanroom facility at the University of New Mexico. The brief fabrication process is demonstrated in Figure 2(a),more details on the fabrication process were described previously[3,21]. The fabrication process of the device involves processing a Silicon on insulator (SOI) wafer with (100) oriented device silicon. SOI wafer had a 25 µm thick device layer and a 350 µm thick handle wafer with 1 µm silicon dioxide buried oxide layer. A 1 µm thick SiO_2 hard mask layer was thermally grown on both sides. The microfabrication process involved performing photolithography to pattern and etch the SiO_2 layer for the nozzles. Plasma etching (RIE) of mask layer (SiO_2) followed by anisotropic etching of the silicon using potassium hydroxide (KOH 35%) at 90°C. The anisotropic etching resulted in a tapered pyramidal shaped nozzle with a highly repeatable 54.74° taper (Figure 1(e)). The KOH concentration and temperature were optimized to reduce surface roughness of the nozzle. The handle silicon was etched using deep reactive ion etching (DRIE) to form the dimensions of the membrane. The buried oxide layer was removed using HF vapor to create the free standing VMA membrane. The silicon membrane was then assembled using the same techniques as the metallic membrane (bonded to metallic washer and PZT ring). The MEMS VMA was designed to operate at similar frequencies and displacements as the metallic VMA. Since silicon is stiffer than stainless steel the thickness of the silicon was significantly lower (25 µm) than the stainless steel (50 µm) in order to maintain similar resonant frequency. The outlet nozzles of the MEMS VMA were also designed to have similar dimensions of 5 and 10 µm as the metallic VMA in order to keep most parameters similar between devices as shown in Figure 2(b, c). The varying parameters were the shape of the nozzle (which is due to the manufacturing process), pitch of the nozzles as MEMS-based devices can have small pitch size due the taper differences, the membrane material (Si vs Stainless Steel), and method of manufacturing resulting in smoother surface. Through the fabrication process the Si-MEMS VMA device had a square outlet nozzle whereas the metallic-VMA had a circular outlet nozzle.

The droplet distribution was measured with a particle size spray analyzer via laser diffraction (Sympatec HELOS KF). Droplet size distribution was determined by analysis of scattered laser light intensity. Initially, all three types of atomizers i.e., ultrasonic, VMA (metallic and MEMS) with orifice diameter 10 µm were tested with DI water. The ultrasonic atomizer was placed 10 cm below the laser beam due to size of the ultrasonic mister and the two VMA were placed 1 cm above the laser beam as it was the optimum place of measurement. Based on the results obtained, the two VMA were selected for further investigation, whereas the ultrasonic device produced both ultrafine (< 1 µm) and large particles (>100 µm) and therefore was not selected for further investigation. Four different liquids with different properties such as DI water, Albuterol, 20% Glycerol, and 10% Cannabidiol water-based liquid isolate (Mile High Labs) were systematically investigated for droplet distribution, VMD, and flow rate for the two VMA devices. The vibration and frequency measurement for the two VMA devices was measured using a MEMS based laser interferometer (Picoscale SmarAct), a non-contact scanning laser-based system to evaluate small-scale displacement as a function of time. The temperature profile of the two VMA was measured using an IR microscope camera (Optris Pi640). The heating rate was determined by measuring the peak temperature across the membrane as a function of time. The viscosity of the liquids was measured using a Cannon-Fenske viscosity tube. The surface tension of the liquids was measured using a Goniometer (Ossila).

Droplet distribution was determined by the width of the distribution calculated by the Span number which is given by:

$$Span = \frac{X_{90} - X_{10}}{X_{50}} \quad (1)$$

Where X_{10}, X_{50} and X_{90} represents droplet size distribution of 10%, 50% and 90% respectively. The Fine particle fraction (FPF) was defined as the fraction of droplets that had sizes between 1 µm and 5 µm. The volume median diameter (VMD) is the midpoint or median droplet size where half of the spray volume are smaller droplets and half are larger droplets.

Results

Initial droplet distribution of three different atomizers (ultrasonic, metallic VMA, and MEMS VMA) were investigated using DI water and the results are demonstrated in Figure 3. Both types of VMA had an outlet nozzle of 10 µm. In the case of ultrasonic device, the X_{10} was 1.71 µm, X_{50} was 123.78 µm and X_{90} was 142.36 µm resulting in a VMD of 90.04 µm. This demonstrates the droplets produced by ultrasonic atomization were either ultra-fine <1 µm or very large >100 µm, representing a very wide distribution. Therefore, the ultrasonic atomization method is not ideal for applications requiring small droplet distribution. The ultrasonic atomization was therefore not further investigated due to the wide droplet distribution and its inability to atomize higher viscosity liquids. The metallic VMA had a droplet distribution where X_{10} was 8.59 µm, X_{50} was 17.10 µm, and X_{90} was 30.68 µm resulting in a VMD of 18.73 µm. The VMD and X_{50} were larger than the outlet nozzle dimension of 10 µm. The MEMS VMA had droplet distribution where X_{10} was 4.30 µm, X_{50} was 7 µm, and X_{90} was 13.64 µm resulting in a VMD of

8.33 μm. Unlike the metallic VMA the VMD and X_{50} of the MEMS-VMA was smaller than the nozzle diameter of 10 μm. Figure 3(c) demonstrates a much narrower distribution compared to the other atomization methods for DI water. Therefore, initial results with DI water demonstrate a significant enhancement in droplet size distribution for the Si-MEMS VMA compared to metallic VMA and ultrasonics. The nozzles of the two VMA devices before any atomization are shown in Figure 1 (d and e). The MEMS-VMA was visually much smoother due to the KOH etching compared to the metallic VMA which resulted in significant residue and surface roughness around the nozzle. The roughness could result in poor surface tension control thus affecting the droplet properties.

Both VMA devices follow a right-skewed normal distribution where the probability density function of a normal random variable is given by

$$f(x|\mu,\sigma^2) = \frac{1}{\sqrt{2\pi\sigma}} e^{-\frac{(x-\mu)^2}{2\sigma^2}}, \quad -\infty < x < \infty, \quad -\infty < \mu < \infty, \qquad \sigma > 0 \tag{2}$$

Where $E(X) = \mu$ and $Var(X) = \sigma^2$.

Dynamics of VMA Devices

The global deformation in the membrane defines the change in micro aperture angle and atomization rate by affecting the volume change at the liquid chamber [25]. The experimental vibration modes corresponding to resonance frequency of various modes are presented in Figure 4 for VMA devices. The frequency spectrum for metallic VMA shows multiple peaks indicating the displacement of the membrane at different frequencies. The first resonant frequency (0,1) mode was observed at 25 kHz followed by the (1,1) mode at 60 kHz. The VMA operates in the (0,2) without liquid and (0,3) mode with a liquid load [26]. The atomization frequency range was thus approximately 93-113 kHz for the metallic VMA. The MEMS VMA was designed to have similar dynamics as the metallic VMA in order to compare device performance without affecting the atomization dynamics. The (0,1) resonant mode was measured at 23 kHz compared to the metallic at 25 kHz. The (0,2) mode was measured at 99 kHz for the MEMS-VMA. The atomization mode for both devices had an operation of approximately 100 kHz. The dynamics of the MEMS-VMA could be easily altered by changing the dimension or thickness of the silicon membrane. Fine tuning of the silicon membrane could be accomplished in the future by controlling the thermally grown oxide thickness which consumes 46% of the silicon. The number of nozzles also slightly affects the stiffness and can be used to fine tune the resonant frequency.

No atomization was observed when the VMA devices were operated in the (0,1) mode, but this mode was used in the ultrasonic device which operated at significantly higher frequency than the VMA. The VMA started to atomize the liquid when the frequency approached the (0,2) mode (~85 kHz) and was maximum between 90 kHz and 102 kHz for the MEMS VMA and near 100 kHz for the metallic VMA. Further increasing the frequency resulted in a significant decrease in atomization as the dynamics changed to the (3,1) mode. The frequency increase from 25 kHz to 100 kHz caused the deformation of the membrane to become complex, which causes the rate of deformation curvature to increase. This

indicates that there was a larger change in the dynamic cone angle which makes the pumping effect stronger and affects atomization rate. Elastic deformation and vibrations of the nozzle membrane allows the micro cone angle to act as pump during the atomization process. Increasing the tapered aperture volume requires more fluid to be pumped in which results in larger and wide range of droplet formation. This is demonstrated by the larger droplet distribution of the metallic VMA compared to the MEMS VMA, as the metallic VMA has a much wider taper than the MEMS VMA (54.74°) as demonstrated in Figure 2(c).

Droplet Size distribution of metallic VMA and MEMS VMA

Table 1 demonstrates the physiochemical properties of the liquids investigated. Each liquid had relatively low viscosity (< 3 cP). The water-based CBD had the lowest density and surface tension but the highest viscosity. Low viscosity liquids were investigated as previous studies have determined that the atomization of metallic VMA were limited to viscosities of <2 cP [18]. However, density and surface tension also have a significant impact on the atomization capability.

Table 1. Physiochemical properties of the liquids used.

Liquid	Density (kg/m^3)	Viscosity (cP)	Surface tension (mN/m)
DI water	997	0.9	72.7
Albuterol	1000	1	72.7
20% Glycerol	1039	1.87	71
10% CBD W-B	807	2.69	53.5

The droplet distribution of the atomized liquids listed in Table 1 from both the metallic and the MEMS VMA devices are shown in Figure 5 (a-d). The MEMS device was operated at 100 kHz and metallic device at 190 kHz with same drive voltage (50 V_{pp}), both devices had an outlet nozzle size of 5 µm, and similar peak displacement. The results of the width of the size distribution (span) and FPF are shown in Table 2. The span of the metallic device was approximately 1 across all liquids with an average span of 1.023, but median droplet size increased as the viscosity increased. The MEMS-VMA device had a significantly lower span with an average of 0.54 for low viscosity (< 2 cP) liquids with no significant change in median droplet size. The span increased for the water-based CBD, which is believed to be due to the increase in viscosity and particles within the liquid. The difference in VMD for both the devices could be explained by their change in volume in the nozzle chamber created by the thin film vibration which depends on oscillation frequency, nozzle diameter and thickness of the membrane [27]. Thickness of the metallic membrane (~50 µm) was thicker than the MEMS device (25 µm) so, with each cycle of the oscillation the metallic VMA pumps and pushes out more liquid than the MEMS VMA, resulting in wide distribution of droplets and larger VMD. The FPF was significantly higher (4.22x, 3.84x, 14.1x, and 15.6x) for the MEMS VMA compared to the metallic VMA for water, Albuterol, 20% Glycerol and 10% CBD respectively. The FPF decreases as the viscosity increases for both devices, but the decrease was less significant with the MEMS-VMA, which means the MEMS-VMA could be better at controlling droplet distribution of higher viscous liquids. The FPF reduces with increased viscosity as larger force are needed to squeeze the higher viscosity liquids through the nozzle, but if the force was constant then droplets increase in size

until the forces can overcome viscosity. The MEMS device has a narrower and more controlled droplet distribution and VMD which was nearly equal to the outlet dimension, resulting in higher FPF. Figure 4 demonstrates that in all cases the MEMS-VMA resulted in enhanced size distribution and smaller VMD when compared to metallic VMA.

Table 2. Comparing Span and FPF for metallic and MEMS VMA devices

Liquids	Span		Fine particle fraction (%)		VMD (μm)	
	Metallic	MEMS	Metallic	MEMS	Metallic	MEMS
DI water	1.06	0.59	22	93	7.6±0.3	5.79±0.4
Albuterol	1.09	0.54	25	96	8.1±0.2	5.82±0.3
20% Glycerol	0.96	0.49	6.1	86	14.37±0.6	5.16±0.5
10% CBD W-B	0.98	1.02	3.52	55	15.72±0.4	5.8±0.6

Liquids with varying fluid properties were investigated to determine the effect of fluid viscosity. For the metallic device, fluid viscosity was inversely proportional to the VMD of the droplets produced which was in good agreement with the results shown previously [28], whereas the MEMS VMA was not significantly affected by the fluid viscosity in regards to the VMD. Even though both devices have the same working principle, frequency, outlet nozzle size, and displacement amplitude, they produced different droplet distribution results with varying liquids. This was believed to be due to i) varying nozzle shape, ii) mechanical properties of silicon compared to stainless steel, and iii) surface roughness. The MEMS VMA produced more uniform droplet sizes and was able to have increased control across a wider range of viscosities. Figure 6 demonstrates the VMD for the two devices with varying liquids. As the viscosity was increased beyond 1 cP, the VMD increased significantly for the metallic VMA whereas the viscosity had little impact on the VMD for the MEMS-VMA. This demonstrates that the MEMS-VMA could potentially atomize higher viscosity liquids with narrow droplet size distribution.

The data from the experiments was statistically analyzed using an ANOVA model. Multiple comparisons were made using Tukey's simultaneous confidence intervals and insights on best performing factor levels was provided. Analysis of the experimental design requires fixed effect 3-factor ANOVA model [29,30]. Device factor was set at 2 levels: (1) MEMS and (2) metallic. Outlet nozzle size diameter was at 4 levels: (1) 5 μm, (2) 10 μm, (3) 20 μm, and (4) 30 μm. Liquid factor was at 4 levels: (1) DI water, (2) albuterol, (3) 20% glycerol and (4) CBD 10% W-B. An additive ANOVA model shown in equation (3) along with the Hasse diagram demonstrated in Figure 7 summarizes the design of experiment.

$$Y_{ijkt} = \mu_{\cdot\cdot} + \alpha_i + \beta_j + \gamma_k + \varepsilon_{ijkt} \quad \text{where } i = \{1, 2\}, j = \{1, 2, 3, 4\}, k = \{1, 2, 3, 4\}, t = \{1, 2, \ldots, 32\}, \sum_{i=1}^{2} \alpha_i = \sum_{j=1}^{4} \beta_j = \sum_{k=1}^{4} \gamma_k = 0, \ \varepsilon \sim iid\ N(0, \sigma^2). \quad (3)$$

Where α_i is the main effect due to i^{th} device, β_j is the main effect of j^{th} hole size, γ_k is the main effect due to k^{th} liquid. Analysis at 5% experimental error demonstrates that i) main effect due to device and outlet nozzle size on VMD are both statistically significant, while the main effect due to liquid was statistically insignificant and ii) metallic device had larger VMD than MEMS-based device. A 95% Tukey's confidence interval (CI) for the difference in metallic VMD and MEMS-based device was (2.79, 7.79). Pairwise comparisons of outlet nozzle size using Tukey's procedure are shown in Table 3.

Table 3. Pairwise comparisons of hole size factor levels. Case 6 implies that hole size of 30 µm produces higher VMD compared to hole size diameter of 20 µm.

Case	Hole size µm	Result	Hole size µm	95% CI for difference
1	10	Higher VMD	5	(0.16, 9.62)
2	20	Higher VMD	5	(9.95, 19.41)
3	30	Higher VMD	5	(22.15, 31.61)
4	20	Higher VMD	10	(5.06, 14.51)
5	30	Higher VMD	10	(17.26, 26.71)
6	30	Higher VMD	20	(7.47, 16.92)

The flow rate of the VMA devices as a function of applied voltage at (0,2) resonance frequency mode was investigated, and the results are shown in Figure 8(a, b). The results demonstrate that as driving voltage increases the flow rate for both devices increase. As voltage increases the peak displacement of the membrane increases from 1.2 µm at 50 V_{pp} to 2.29 µm at 100 V_{pp}. As the mesh membrane deformation increases the variation in the tapered volume exerts more pumping effect leading to higher atomization rates. The flow rate of DI water and albuterol was 50±2 µL/min at 50 V_{pp} for both devices and reaches 170±5 µL/min for metallic VMA and 130±5 µL/min for MEMS VMA at 100 V_{pp}. The flow rates for 20% glycerol were 30±3 µL/min for both devices at 50 V_{pp} and reaches 120±3.5 µL/min for metallic VMA and 80±3.5 µL/min for the MEMS VMA at 100 V_{pp}. For 10% CBD, the flow rate was reduced to 24±1 µL/min at 40 V_{pp} and increased to 75±2 µL/min for metallic device and 54±3 µL/min for the MEMS VMA. The flow rate of low viscosity, low density liquid was the same for both the devices at low voltages but at higher voltages the metallic VMA had slightly higher flow rate (~30 µL/min) because the droplet distribution was wider, and the droplets produced were larger in size in comparison to the MEMS VMA. The increased liquid viscosity resulted in decreased flow rate for both devices.

Based on the results the MEMS VMA demonstrated significantly enhanced droplet distribution, VMD, and FPF for various liquids with different physiochemical properties. The MEMS VMA was selected for further investigation to determine effects of varying the outlet nozzle diameter, pitch of the inlet nozzles and distance of measurement from the laser source on droplet distribution. The outlet diameter was varied by changing the mask dimensions, but the taper remained the same. The various outlet nozzles investigated had dimensions of 4 µm, 6 µm, 8 µm, and 10 µm. The droplet distribution and VMD of the varying outlet dimensions of the MEMS VMA are shown in Figure 9(a). The distribution curve shifts to the left (smaller) as the outlet nozzle was reduced. The peak value of the distribution curve had similar size as the outlet nozzle dimensions. The 4 µm nozzle had a VMD of 4.53 µm and as the nozzle diameter increases the distribution curve shifts away from the axis. Figure 9(b) demonstrates the VMD as a function of outlet nozzle, which demonstrates a linear relationship for various liquids. The VMD value was in range of

4.53±0.4 µm to 5.43±0.4 µm for the 4 µm nozzle size, 6.08±0.5 µm to 6.46±0.5 µm for 6 µm size, 7.92±0.3 to 8.91±0.3 µm for 8 µm size, 9.23±0.5 µm to 11.2±0.4 µm for 10 µm size. This demonstrates that as outlet nozzle increases the distribution of the VMD becomes wider along with an increase in VMD size. Therefore, the MEMS VMA device was able to have a narrower droplet size distribution, as the outlet nozzle dimensions can be very accurately produced with high repeatability, as it is dependent on the anisotropic etching of silicon for which the taper depends on the crystal planes. The (100) crystal plane intersects the (111) plane at (54.74°) which was the angle of the taper, because the KOH etching of the (111) plane was about 200x slower. Thus, the taper of (100) Si will always produce a 54.74° taper, so by altering the mask dimensions the outlet nozzle can be accurately predicted.

The effects of nozzle pitch on distribution were investigated for the MEMS VMA device with 4 µm nozzle size and the results are shown in Figure 10(a). The results demonstrate that the device with 60 µm pitch had narrow distribution with span of 0.63. The distribution widens as the pitch was increased to 90 µm and 120 µm with a span of 1.16 and 1.2 respectively. This agrees with the metallic VMA devices which had a larger span and larger pitch than the Si-VMA. Nozzle pitch was also directly related to the number of nozzles on the membrane as lower pitch values correspond to more holes (4000 holes for 60 µm pitch) compared to 2000 and 1000 holes for 90 µm and 120 µm pitch. The distance of VMA to the laser on the particle analyzer results in varying VMD as demonstrated in Figure 10(b). If the VMA was positioned close to the laser, the VMD results were lower than if the device was positioned approximately 30 mm away. This was likely due to coalescing of multiple small droplets resulting in large droplet formation.

Temperature Distribution

Temperature of the membrane through friction and piezoelectric material can affect the liquid properties and lead to degradation of the liquid or change the chemical composition of the liquid, so controlling temperature can be important for atomizing various liquids. Average temperature distribution across the membrane of the two VMA devices was investigated at a driving voltage of 50 V_{pp}, and the results are shown in Figure 11(a-c). The heat from the piezoelectric actuation causes a significant increase in the metallic VMA, which reached an average temperature of 87.9°C in about 40 s. This is significantly higher than the heating of the MEMS VMA (34.6°C) for the same duration. This was believed to be due to the difference in thermal conductivity of the two materials and to the bonding mechanism. The heat transfer rate was demonstrated in Figure 11(c). Increased surface temperature for the atomizer device can affect the liquid as it may react and deteriorate the physical and chemical properties, therefore the use of metallic VMA may not be suitable for certain liquids and applications as it could lead to degradation of the liquid. The heating in the metallic VMA was less controllable and predictable compared to the MEMS VMA.

Conclusion

This study investigated three types of atomizers including ultrasonic, metallic VMA and MEMS VMA and the results demonstrate that the ultrasonic device produces a wide range of droplet sizes and was not

able to atomize higher viscosity liquids, which agrees with previous research. The two VMA devices were compared dynamically to have similar frequency modes and displacement with applied voltages. However, the material, thickness, nozzle shape, outlet nozzle shape, and surface roughness varied between VMA devices. These variations lead to statistically significant affects on droplet size and distribution and device performance.

Droplet distribution for VMA devices followed a right-skewed normal distribution. A range of fluids with different physiochemical properties were atomized using the metallic and MEMS VMA. The aerosol performance including droplet size distribution, VMD, and output rate were dependent on fluid characteristics for both VMA devices. Regardless of the fluid the metallic VMA generated aerosols with wider distribution, larger VMD, and smaller FPF than MEMS VMA. For MEMS VMA, droplet size did not change with varying viscosity, but the output rate was decreased due to flow resistance. The flow rates were significantly reduced for higher viscosity liquids in both devices. After comparing the two devices, further study on MEMS VMA was carried out to study the effect of outlet nozzle size, pitch, and measurement distance from laser source on the VMD. Outlet nozzle size and median drop size follows a linear relationship for all the liquids tested and average drop size corresponded to the size of the outlet nozzle. Therefore, creating a device with a specific droplet size is feasible with the MEMS VMA. Since the MEMS VMA was fabricated in a cleanroom environment it has the ability to be customized, thus pitch size of the nozzles could be varied. Varying the pitch size of the nozzles resulted in varying the density of nozzles on the membrane, and it was observed that a large array of nozzles resulted in enhanced density distribution. This study has shown that both VMA devices are not only affected by the fluid properties, but also these perform differently due to their design and dimensions despite the same working principle and dynamics. The ability to easily customize dimensions, including nozzle dimensions using microfabrication techniques offer unique advantages to the MEMS VMA over metallic VMA.

Declarations

Acknowledgements:

The authors would like to thank the members of the Manufacturing Training and Technology Center (MTTC) at the University of New Mexico for their help. This research was funded by the STC UNM Gap Fund and the Research Allocation Committee Grant from University of New Mexico.

Author Contributions:

PS: Is the first author who had the responsibility of manufacturing the devices as well as leading efforts in the experimentation and writing of the manuscript.

MQ: Was responsible for the statistical analysis.

IV: Helped PS with the experimentation of the droplet analysis data.

NJ: Is the PI for the project and was responsible for funding the research, editing the paper, and advising on experimentation and analysis.

Additional Information

The authors declare no competing interests.

References

1 Djupesland, P. G. Nasal drug delivery devices: characteristics and performance in a clinical perspective—a review. *Drug Delivery and Translational Research***3**, 42-62, doi:10.1007/s13346-012-0108-9 (2013).

2 Li, Q. *et al.* Additive Mixing and Conformal Coating of Noniridescent Structural Colors with Robust Mechanical Properties Fabricated by Atomization Deposition. *ACS Nano***12**, 3095-3102, doi:10.1021/acsnano.7b08259 (2018).

3 Sharma, P. & Jackson, N. Vibrating Mesh Atomizer for Spin-Spray Deposition. *Journal of Microelectromechanical Systems***30**, 582-588, doi:10.1109/JMEMS.2021.3092966 (2021).

4 Sharma, P. & Jackson, N. in *2021 IEEE 34th International Conference on Micro Electro Mechanical Systems (MEMS)*. 681-684.

5 Beck-Broichsitter, M., Paulus, I. E., Greiner, A. & Kissel, T. Modified vibrating-mesh nozzles for advanced spray-drying applications. *European Journal of Pharmaceutics and Biopharmaceutics***92**, 96-101, doi:https://doi.org/10.1016/j.ejpb.2015.03.001 (2015).

6 Kiontke, A. *et al.* Surface acoustic wave nebulization improves compound selectivity of low-temperature plasma ionization for mass spectrometry. *Scientific Reports***11**, 2948, doi:10.1038/s41598-021-82423-w (2021).

7 Dolovich, M. B. & Dhand, R. Aerosol drug delivery: developments in device design and clinical use. *The Lancet***377**, 1032-1045, doi:10.1016/S0140-6736(10)60926-9 (2011).

8 Lake, J. R. The effect of drop size and velocity on the performance of agricultural sprays. *Pesticide Science***8**, 515-520, doi:https://doi.org/10.1002/ps.2780080514 (1977).

9 Dombrowski, N., Fraser, R. P. & Newitt, D. M. A photographic investigation into the disintegration of liquid sheets. *Philosophical Transactions of the Royal Society of London. Series A, Mathematical and Physical Sciences***247**, 101-130, doi:doi:10.1098/rsta.1954.0014 (1954).

10 Chen, B. *et al.* Investigation of the droplet characteristics and size distribution during the collaborative atomization process of a twin-fluid nozzle. *The International Journal of Advanced Manufacturing Technology***107**, 1625-1639, doi:10.1007/s00170-020-05131-1 (2020).

11 Wittner, M. O., Karbstein, H. P. & Gaukel, V. Pneumatic Atomization: Beam-Steering Correction in Laser Diffraction Measurements of Spray Droplet Size Distributions. *Applied Sciences***8**, 1738 (2018).

12 Zhang, Y., Yuan, S. & Wang, L. Investigation of capillary wave, cavitation and droplet diameter distribution during ultrasonic atomization. *Experimental Thermal and Fluid Science***120**, 110219, doi:https://doi.org/10.1016/j.expthermflusci.2020.110219 (2021).

13 Wang, W.-N. *et al.* Investigation on the Correlations between Droplet and Particle Size Distribution in Ultrasonic Spray Pyrolysis. *Industrial & Engineering Chemistry Research***47**, 1650-1659, doi:10.1021/ie070821d (2008).

14 Kooij, S., Astefanei, A., Corthals, G. L. & Bonn, D. Size distributions of droplets produced by ultrasonic nebulizers. *Scientific Reports***9**, 6128, doi:10.1038/s41598-019-42599-8 (2019).

15 Rajan, R. & Pandit, A. B. Correlations to predict droplet size in ultrasonic atomisation. *Ultrasonics***39**, 235-255, doi:https://doi.org/10.1016/S0041-624X(01)00054-3 (2001).

16 Tsai, S. C. *et al.* High-frequency, silicon-based ultrasonic nozzles using multiple Fourier horns. *ieee transactions on ultrasonics, ferroelectrics, and frequency control***51**, 277-285 (2004).

17 Alvarez, M., Friend, J. & Yeo, L. Y. Rapid generation of protein aerosols and nanoparticles via surface acoustic wave atomization. *Nanotechnology***19**, 455103 (2008).

18 Ghazanfari, T., Elhissi, A. M., Ding, Z. & Taylor, K. M. The influence of fluid physicochemical properties on vibrating-mesh nebulization. *International journal of pharmaceutics***339**, 103-111 (2007).

19 Choi, K.-H. *et al.* Fabrication and characterization of medical mesh-nebulizer for aerosol drug delivery. *Applied Sciences***8**, 604 (2018).

20 Jackson, N., Mathewson, A. & Olszewski, Z. (Google Patents, 2020).

21 Olszewski, O. Z. *et al.* A silicon-based MEMS vibrating mesh nebulizer for inhaled drug delivery. *Procedia Engineering***168**, 1521-1524 (2016).

22 Yan, Q., Sun, W. & Zhang, J. Study on the Influencing Factors of the Atomization Rate in a Piezoceramic Vibrating Mesh Atomizer. *Applied Sciences***10**, 2422 (2020).

23 Yan, Q., Wu, C. & Zhang, J. Effect of the Dynamic Cone Angle on the Atomization Performance of a Piezoceramic Vibrating Mesh Atomizer. *Applied Sciences***9**, 1836 (2019).

24 Moon, S.-H. *et al.* Effects of Driving Frequency and Voltage on the Performances of Vibrating Mesh Nebulizers. *Applied Sciences***11**, 1296 (2021).

25 Cai, Y., Zhang, J., Zhu, C., Huang, J. & Jiang, F. Theoretical calculations and experimental verification for the pumping effect caused by the dynamic micro-tapered angle. *Chinese Journal of Mechanical*

*Engineering***29**, 615-623, doi:10.3901/CJME.2016.0324.037 (2016).

26 Houlihan, R., Timothy, M., Duffy, C., MacLoughlin, R. & Olszewski, O. in *2021 21st International Conference on Solid-State Sensors, Actuators and Microsystems (Transducers).* 615-618 (IEEE).

27 Guerra-Bravo, E., Lee, H.-J., Baltazar, A. & Loh, K. J. Vibration Analysis of a Piezoelectric Ultrasonic Atomizer to Control Atomization Rate. *Applied Sciences***11**, 8350 (2021).

28 Ghazanfari, T., Elhissi, A. M. A., Ding, Z. & Taylor, K. M. G. The influence of fluid physicochemical properties on vibrating-mesh nebulization. *International Journal of Pharmaceutics***339**, 103-111, doi:https://doi.org/10.1016/j.ijpharm.2007.02.035 (2007).

29 Dean, A. M. & Voss, D. *Design and Analysis of Experiments*. (Springer New York, 2000).

30 Kutner, M. H., Neter, J., Nachtsheim, C.J. and Li, W. .

Applied Linear Regression Models (2004).

Figures

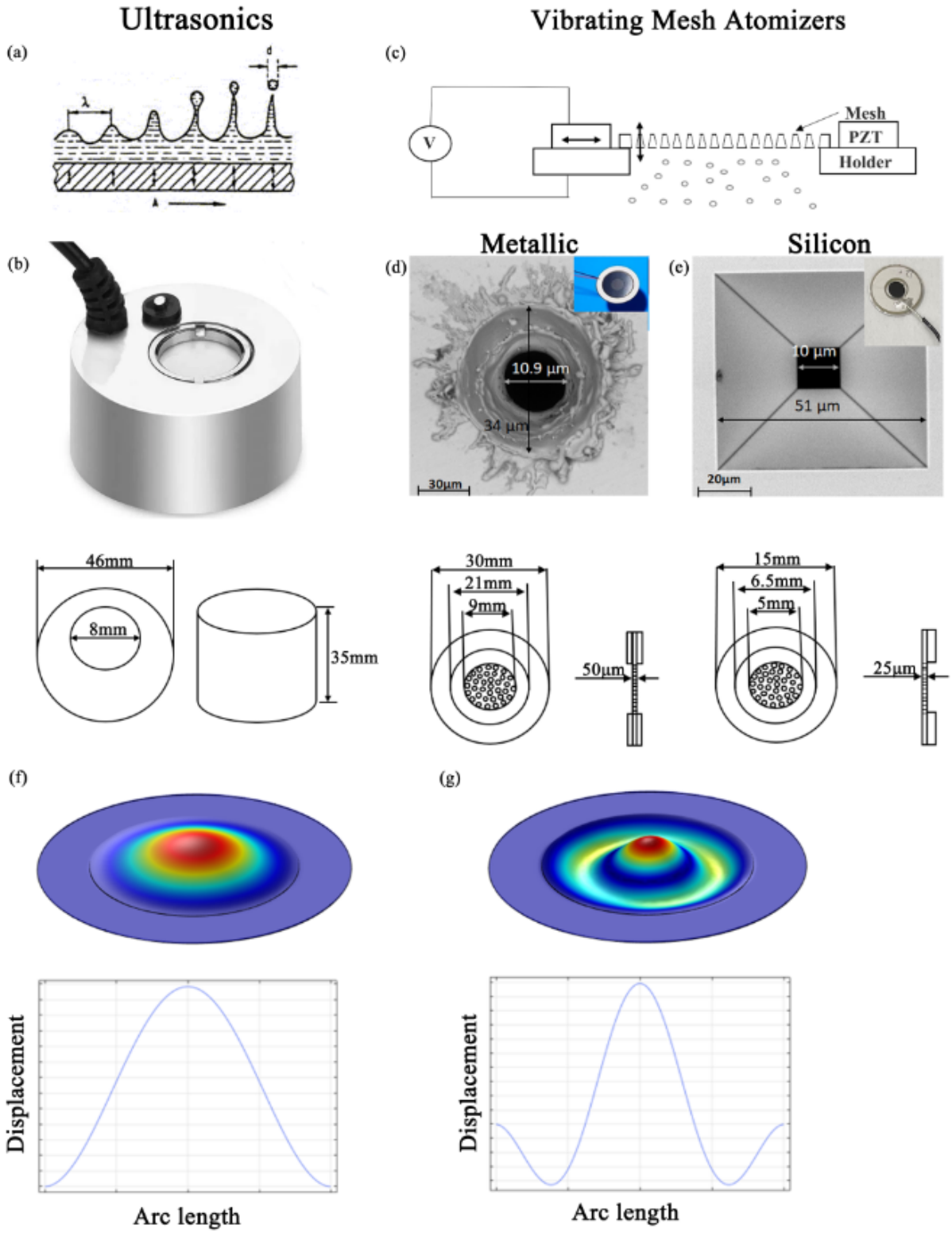

Figure 1

Atomizer type investigated. (a, b) Working principle of ultrasonic mist maker and device image, (c) Working principle of vibrating mesh atomizer, (d & e) SEM top view image of single nozzle (d) Metallic VMA (e) MEMS VMA, Vibration mode of (f) ultrasonic device (0,1) and (g) (0,2) .

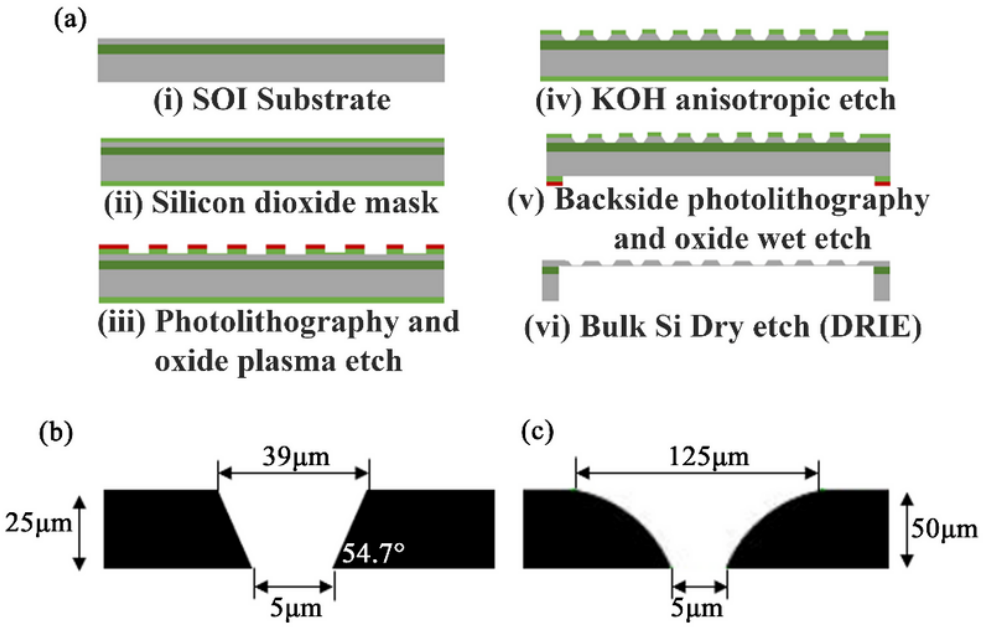

Figure 2

(a) Schematic of the fabrication steps of MEMS VMA, Nozzle outlet shape of (b) MEMS VMA and (c) Metallic VMA.

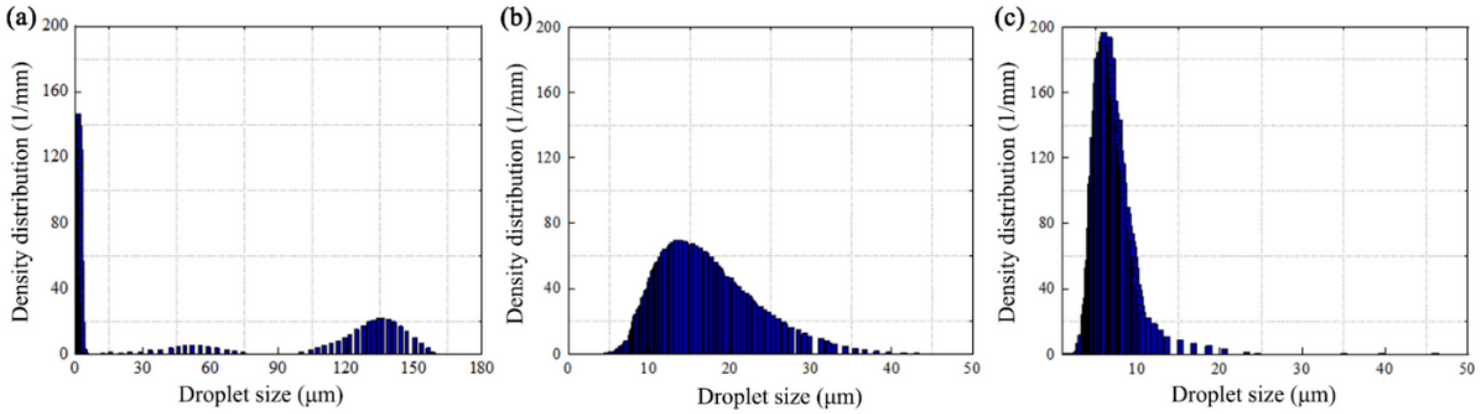

Figure 3

DI water droplet distribution by devices (a) ultrasonic device, (b) Metallic VMA and (c) MEMS VMA

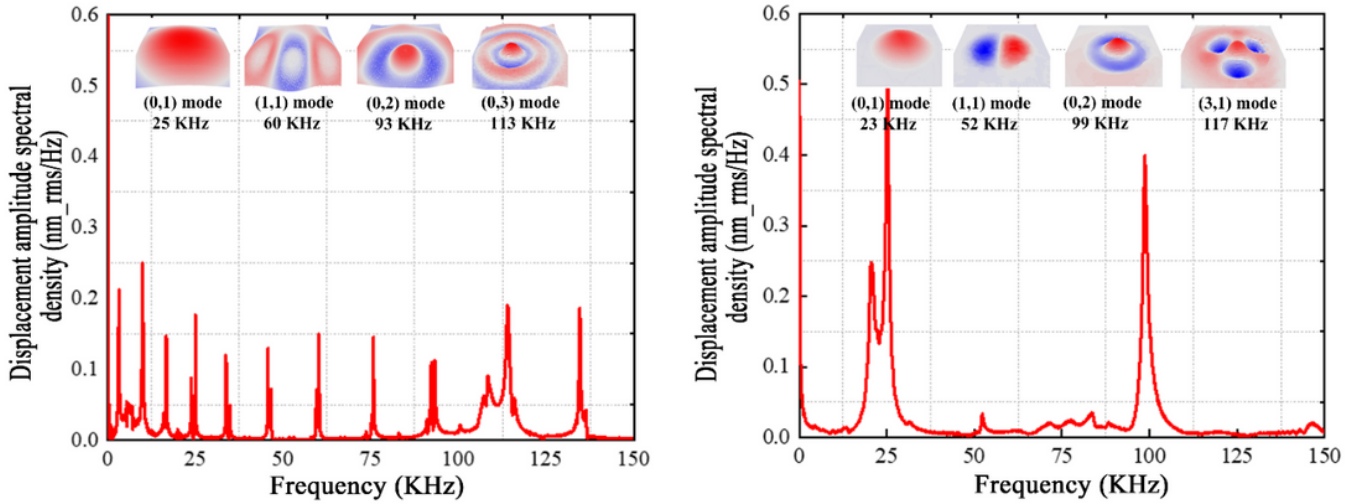

Figure 4

Frequency spectrum of (a) Metallic VMA, (b) MEMS VMA

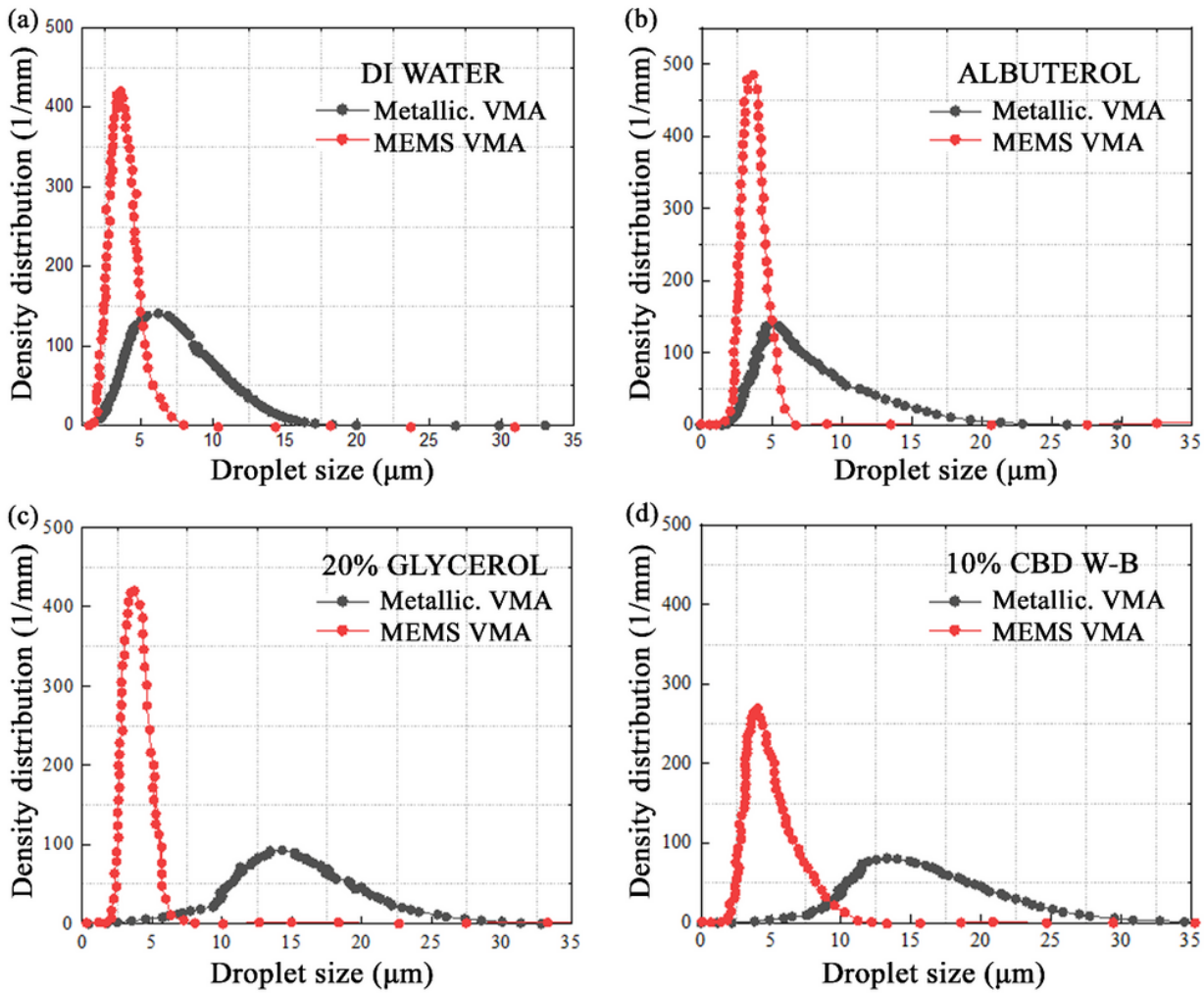

Figure 5

Droplet distribution for Metallic and MEMS VMA for (a) DI water, (b) Albuterol, (c) 20% Glycerol and (d) 10% CBD Water-based.

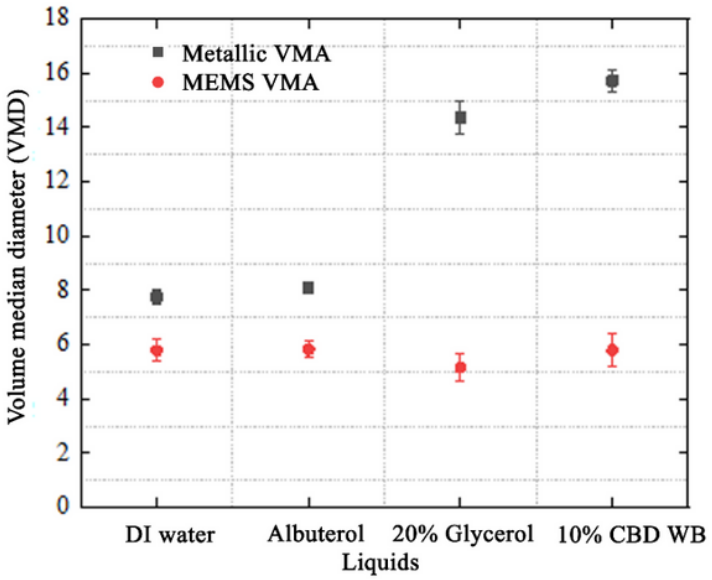

Figure 6

VMD of two devices used for DI water, Albuterol, 20% Glycerol and 10% CBD W-B.

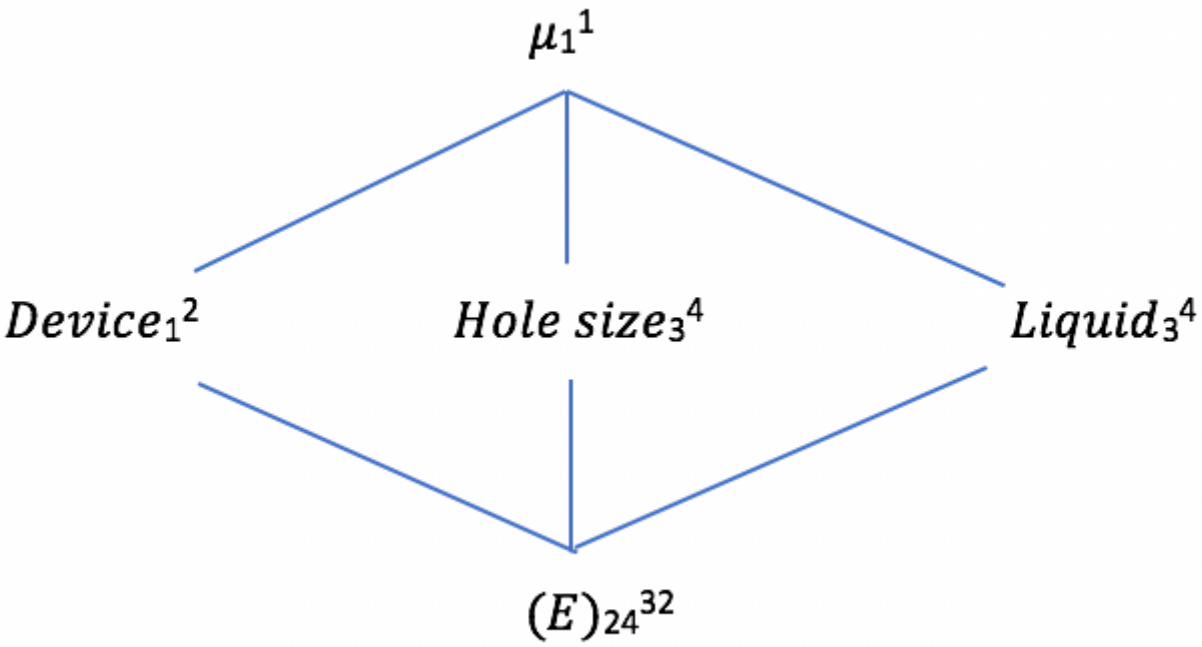

Figure 7

Hasse diagram for VMD experiment.

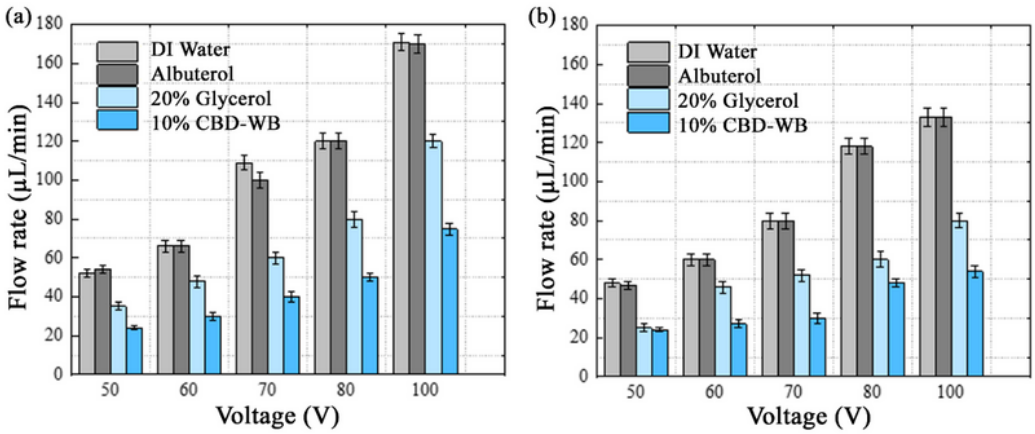

Figure 8

Flow rate of (a) Metallic VMA and (b) MEMS VMA.

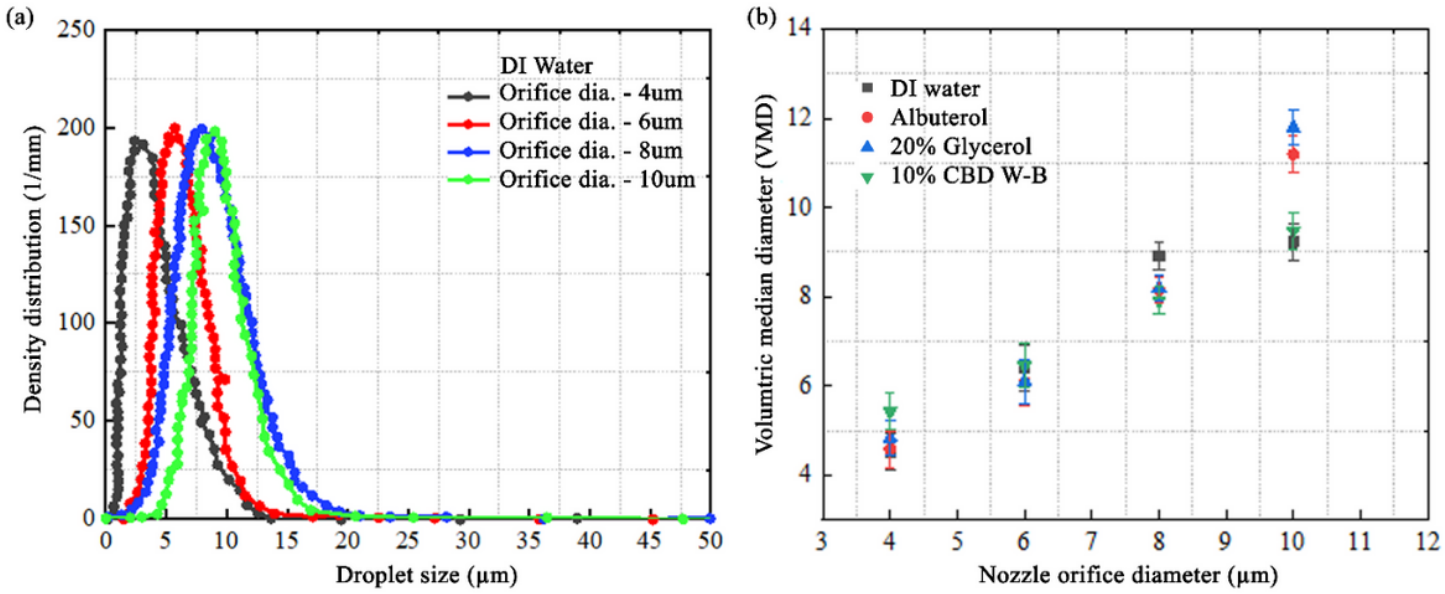

Figure 9

Effect of orifice outlet diameter on (a) Droplet distribution and (b) VMD.

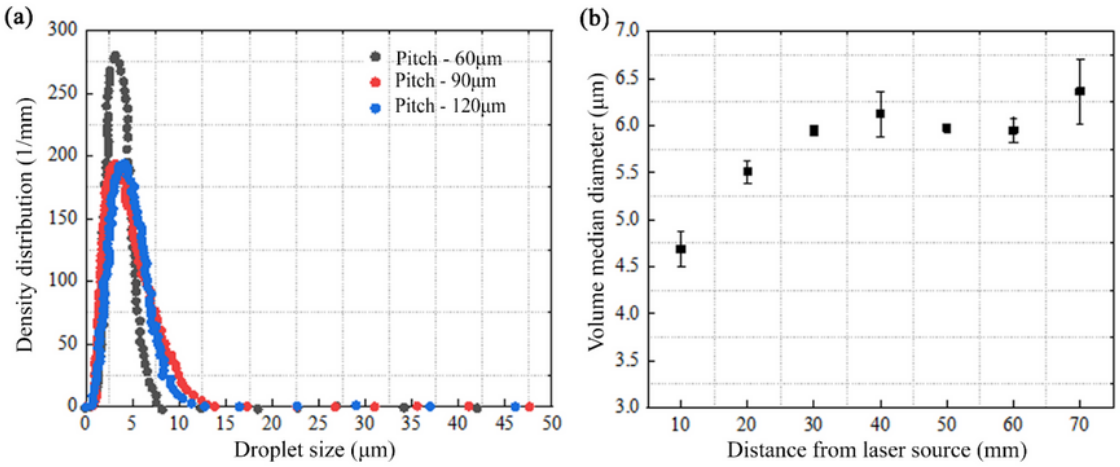

Figure 10

(a) Effect of hole pitch on the droplet distribution, (b) Distance of device from laser source on VMD.

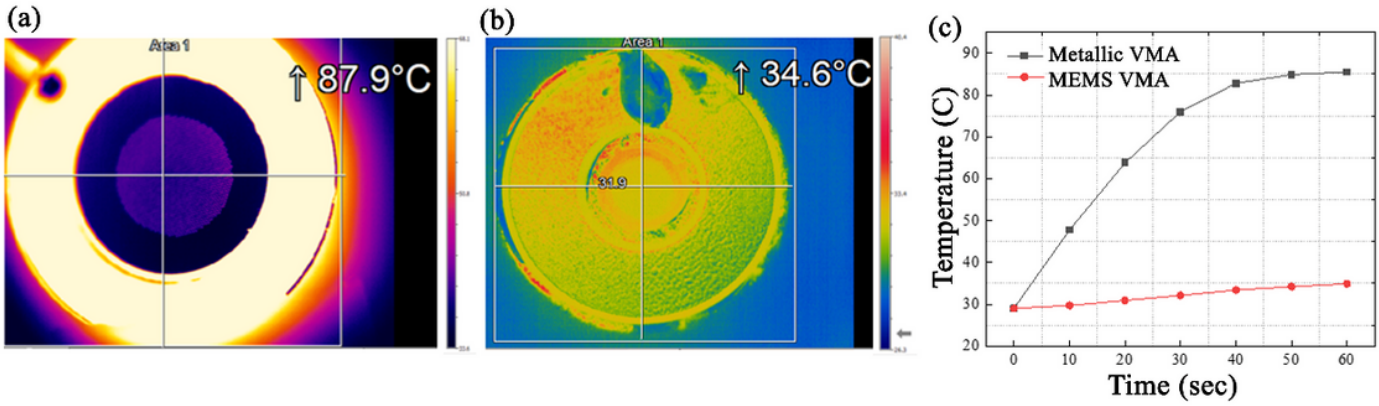

Figure 11

Surface temperature of (a) metallic VMA, (b) MEMS VMA, (c) Time temperature for both the device after 1 minute of operation.